

Galloping and spinning modes of subsonic detonation

I Brailovsky[†], M Frankel[‡] and G Sivashinsky^{†§}

[†] School of Mathematical Sciences, Tel Aviv University, Ramat Aviv, Tel Aviv 69978, Israel

[‡] Department of Mathematical Sciences, Indiana University–Purdue University, Indianapolis, IN 46202, USA

[§] The Levich Institute for Physico-Chemical Hydrodynamics, The City College of New York, New York, NY 10031, USA

Received 24 April 1999, in final form 10 January 2000

Abstract. A reduced model for a pressure-driven subsonic combustion wave spreading through an inert porous medium (subsonic detonation) is derived. It is shown that the associated planar travelling wave solution may lose its stability assuming a galloping or spinning structure as occurs in supersonic free-space detonation. The problem of subsonic detonation is found to be dynamically akin to the problem of glassless combustion known for its rich pattern-forming dynamics.

1. Introduction

It has long been observed that the presence of obstacles (tube walls, wire screens, solid particles, porous medium matrix, etc) may have a profound effect on premixed gas combustion. Apart from inducing hydrodynamic and thermal disturbances and thereby affecting the combustion wave speed, the obstacles also exert resistance to the gas flow causing reduction of its momentum. As has recently been realized the loss of momentum (drag) is of direct relevance to the explosive transition from deflagration to detonation and also to the hysteretic transition from supersonic sub-CJ detonation (quasi-detonation) to the pressure-driven subsonic combustion wave dominated by convective effects [1, 2]. The latter regime which may be referred to as ‘subsonic detonation’ is the main concern of the current study.

Perhaps the geometrically and physically simplest and yet experimentally quite feasible [3] system for studying subsonic detonation is premixed gas combustion within an inert porous medium. In this case, on one hand, the distortions introduced by the porous matrix may be ignored while, on the other hand, the resistance of the matrix to the gas flow is often so strong that one may neglect the inertial effects and take Darcy’s law as the momentum equation. In this high-drag limit shocks are ruled out and the pressure non-uniformities are equalized not by the acoustic waves but rather through diffusion of pressure associated with low Reynolds number creeping flows. For many gas–porous medium systems the gas pressure diffusivity exceeds its thermal diffusivity by several orders of magnitude, thereby emerging as the principal transport agency controlling the reaction spread.

It is well known that the steady one-dimensional profile of conventional CJ detonation may easily lose its stability assuming a galloping or spinning structure. As will be shown below, similar bifurcation is typical of subsonic detonation as well. Unlike the former, however, the subsonic detonation (due to its predominantly diffusive nature) constitutes rather a benign dynamical system, which is advantageous both for analytical and numerical explorations. Moreover, in a certain parameter range the problem of subsonic detonation

becomes functionally identical to the problem of gasless combustion (self-propagating high-temperature synthesis) known for its rich pattern-forming dynamics involving, among other things, galloping and spinning structures as well as period-doubling cascades and chaos [4–7].

2. Model

To single out the impact of momentum loss the effective features of the reactive gas–porous medium system will be assumed to be controlled exclusively by its gaseous phase subject to the resistance of the porous medium matrix. The thermal and molecular diffusivities will be regarded as negligibly small (compared to the barodiffusivity) which indeed holds for many real-world systems. As an additional simplification the so-called small-heat-release (SHR) approximation will be employed where variations of temperature, pressure, density and gas velocity are regarded as small and, hence, the nonlinear effects are ignored everywhere except in the reaction rate term, which is generally highly sensitive even to minor temperature changes. In this formulation the problem becomes much more tractable mathematically, while presumably preserving some basic features of the original fully nonlinear system. In a non-dimensional formulation the resulting model reads

$$\gamma\Theta_\tau - (\gamma - 1)\Pi_\tau = \Omega(\Phi, \Theta) \quad (2.1)$$

$$\Phi_\tau = -\Omega(\Phi, \Theta) \quad (2.2)$$

$$\Pi_\tau - \Theta_\tau = \nabla^2\Pi \quad (2.3)$$

$$\Omega(\Phi, \Theta) = A\Phi \exp(-N/(\sigma + (1 - \sigma)\Theta)). \quad (2.4)$$

Equations (2.1) and (2.2) represent the partially linearized conservation equations for energy and the deficient reactant. Equation (2.3) is a linearized continuity equation, incorporating the equations of state and momentum (Darcy’s law). A detailed derivation is presented in [8] (see also [9]).

Prior to ignition,

$$\Theta = 0 \quad \Pi = 0 \quad \Phi = 1. \quad (2.5)$$

Here $\Theta = (T - T_0)/(T_\infty - T_0)$, $\Pi = (P - P_0)/(P_\infty - P_0)$, $\Phi = C/C_0$, $\Omega = W/W_\infty$, $(\xi, \eta, \zeta) = (x, y, z)/x_\infty$, $\tau = t/t_\infty$, are the scaled temperature (Θ), pressure (Π), deficient reactant concentration (Φ), reaction rate (Ω) and spatio-temporal coordinates (ξ, η, ζ, τ) ; $\nabla^2 = \partial_{\xi\xi} + \partial_{\eta\eta} + \partial_{\zeta\zeta}$. T_0, P_0, C_0, ρ_0 are the dimensional temperature, pressure, concentration and gas density prior to ignition. T_∞, P_∞ are the final temperature and pressure of combustion products reached upon adiabatic homogeneous explosion. $W_\infty = A^{-1}ZC_0\rho_0$, $t_\infty = C_0\rho_0/W_\infty$, $x_\infty = \sqrt{D_b t_\infty}$ are the reaction rate and spatio-temporal scales. $D_b = Ka_0^2/\gamma\nu$ is the barodiffusivity; K the porous medium permeability; $a_0 = \sqrt{\gamma(c_p - c_v)T_0}$ the speed of sound; ν the kinematic viscosity; $\gamma = c_p/c_v$; $\sigma = T_0/T_\infty$; $N = E/R^0T_\infty$ the scaled activation energy (E); R^0 the universal gas constant; $A = A(N, \gamma, \sigma)$ is a normalizing factor, to keep the reaction wave velocity near unity. For large N , as suggested in the recent analysis by Goldfarb *et al* [10] adapted for the present SHR case,

$$A = (1 - \gamma^{-1}) \exp(N/(\sigma + (1 - \sigma)(1 - \gamma^{-1}))). \quad (2.6)$$

An independent numerical validation of this relation is given in the appendix.

In the high-activation-energy limit ($N \rightarrow \infty$) the reaction zone shrinks, turning the reaction rate term (Ω) into a localized source distributed along an interface, $F(\xi, \eta, \zeta, \tau) = 0$.

This limit does not destroy continuity of the pressure (Π). Yet, due to the absence of molecular and thermal diffusivities disregarded in the model, the concentration (Φ) and temperature (Θ) fields vary in a discontinuous manner. Analysis of the basic travelling wave solution (see the appendix) shows that at large N the bulk of the reaction is associated with the temperature at the entrance to the reaction zone, suggesting the following approximation for the reaction rate term:

$$\Omega \simeq Q\delta_F \quad (2.7)$$

where δ_F is the surface delta-function and

$$Q = \exp(-N/2(\sigma + (1 - \sigma)\Theta_+)) \exp(N/2(\sigma + (1 - \sigma)\Theta_+^{(0)})). \quad (2.8)$$

Θ_+ is the gas temperature on the unburnt (+) side of the interface,

$$\Theta_+^{(0)} = 1 - \gamma^{-1} \quad (2.9)$$

its value for the planar uniformly propagating flame [8].

In the burnt gas region (-), where the deficient reactant is completely consumed, $\Phi = 0$.

Equations (2.1) and (2.2) readily imply

$$\gamma\Theta - (\gamma - 1)\Pi + \Phi = \Psi(\xi, \eta, \zeta) \quad (2.10)$$

where Ψ is defined by the initial conditions. In keeping with the pre-ignition condition (2.5), it will be assumed that $\Psi = 1$ beyond some finite domain.

In the course of time one may thus set

$$\gamma\Theta - (\gamma - 1)\Pi + \Phi = 1. \quad (2.11)$$

Applying this relation to the burnt (-) and unburnt (+) sides of the interface and recalling that $\Phi_- = 0$, $\Phi_+ = 1$, one readily finds

$$\Theta_- = \Theta_+ + \gamma^{-1} \quad (2.12)$$

$$\Theta_+ = 1 + (1 - \gamma^{-1})(\Pi - 1) \quad (2.13)$$

where, due to the pressure continuity, $\Pi = \Pi_- = \Pi_+$.

Substituting (2.9), (2.12) and (2.13) into (2.8), after some simple algebra one obtains

$$Q = \exp(\alpha(\Pi - 1)/(\Sigma + (1 - \Sigma)\Pi)) \quad (2.14)$$

where

$$\alpha = \frac{N(1 - \sigma)(1 - \gamma^{-1})}{2(1 - \gamma^{-1}(1 - \sigma))^2} \quad (2.15)$$

and

$$\Sigma = (\gamma\sigma)/(\gamma - 1 + \sigma) \quad (\Sigma < 1). \quad (2.16)$$

Combining equations (2.1) and (2.3) to eliminate Θ_τ one finally ends up with the formulation expressed entirely in terms of the pressure (Π) and concentration (Φ),

$$\Pi_\tau = \gamma\nabla^2\Pi + Q(\Pi)\delta_F \quad (2.17)$$

$$\Phi_\tau = -Q(\Pi)\delta_F. \quad (2.18)$$

Setting

$$\tau = \gamma\hat{\tau} \quad (\xi, \eta, \zeta) = \gamma(\hat{\xi}, \hat{\eta}, \hat{\zeta}) \quad (2.19)$$

the system (2.17) and (2.18) becomes

$$\Pi_{\hat{t}} = \hat{\nabla}^2 \Pi + Q(\Pi) \delta_{\hat{f}} \quad (2.20)$$

$$\Phi_{\hat{t}} = -Q(\Pi) \delta_{\hat{f}} \quad (2.21)$$

involving only two independent parameters, α and Σ .

Here $\hat{\nabla}^2$ and $\delta_{\hat{f}}$ are associated with the modified coordinates $(\hat{\xi}, \hat{\eta}, \hat{\zeta})$.

Equations (2.20) and (2.21) should be considered jointly with the conditions

$$\Pi \rightarrow 0 \quad \text{far ahead of the advancing interface} \quad (2.22)$$

$$\Phi \equiv 1 \quad \text{ahead of the interface} \quad \text{and} \quad \Phi \equiv 0 \quad \text{behind.} \quad (2.23)$$

The resulting model, interestingly enough, is formally identical to the free-interface model for gasless combustion (self-propagating high-temperature synthesis) if Π is regarded as the scaled temperature; 2α , the Zeldovich number and Σ , the unburnt/burnt phase temperature ratio. In this context the model has been explored energetically in recent years and there is a sizeable volume of analytical and numerical results on its intrinsic dynamics (see, e.g., [7] and references therein).

The reduced models (2.1)–(2.4) and (2.17), (2.18) correspond to the small Mach number limit ($M = x_{\infty}/a_0 t_{\infty} \ll 1$). This, however, does not imply that the pressure variation is also small as occurs in free-space deflagrations. In porous media, due to friction, the gas velocity (in the frame of reference attached to the matrix) vanishes both far ahead of the reaction zone and behind it. Hence, as readily follows from the continuity equation, the density of the burnt gas returns to its initial value. As a result, the final pressure of the combustion products is identical to that reached in the constant-volume adiabatic explosion. The pressure variation is small only on length scales comparable to the reaction zone width. Moreover, similarly to the conventional free-space deflagration there is a small pressure drop, $\Delta P/(P_{\infty} - P_0) \sim M^2$, throughout the reaction zone [2]. The latter effect, however, is not covered by the current model, pertinent to the leading-order small Mach number asymptotics.

3. Basic propagation mode and its stability

In this section we briefly recall the main facts on the structure and stability of the basic travelling wave solution corresponding to a planar uniformly propagating detonation. Assuming

$$\Pi = \Pi^{(0)}(\hat{\xi} - \lambda \hat{t}) \quad \Phi = \Phi^{(0)}(\hat{\xi} - \lambda \hat{t})$$

one easily finds that the associated boundary value problem has a unique solution

$$\begin{aligned} \Pi^{(0)} &= \exp(-\hat{\xi} + \lambda \hat{t}) & \Phi^{(0)} &= 1 & \text{at } \hat{\xi} > \lambda \hat{t} \\ \Pi^{(0)} &= 1 & \Phi^{(0)} &= 0 & \text{at } \hat{\xi} < \lambda \hat{t} \quad \text{where } \lambda = 1. \end{aligned} \quad (3.1)$$

The linear stability analysis of (3.1) leads to the following dispersion relation [11]:

$$4\omega^3 + (1 + 4k^2 + 4\alpha - \alpha^2)\omega^2 + (\alpha + 4\alpha k^2)\omega + \alpha^2 k^2 = 0 \quad (3.2)$$

involving a single parameter, α .

Here ω is the instability increment; $k = |\mathbf{k}|$, where \mathbf{k} is the wavevector of the harmonic perturbation in $\hat{\eta}$ and $\hat{\zeta}$.

For the marginal stability curve ($\text{Re } \omega = 0$) (3.2) yields (figure 1)

$$k = \kappa_{\pm}(\alpha) = \frac{1}{4} \sqrt{2(\alpha^2 - 3\alpha - 2 \pm \sqrt{\alpha^4 - 6\alpha^3 + 9\alpha^2 - 4\alpha})}. \quad (3.3)$$

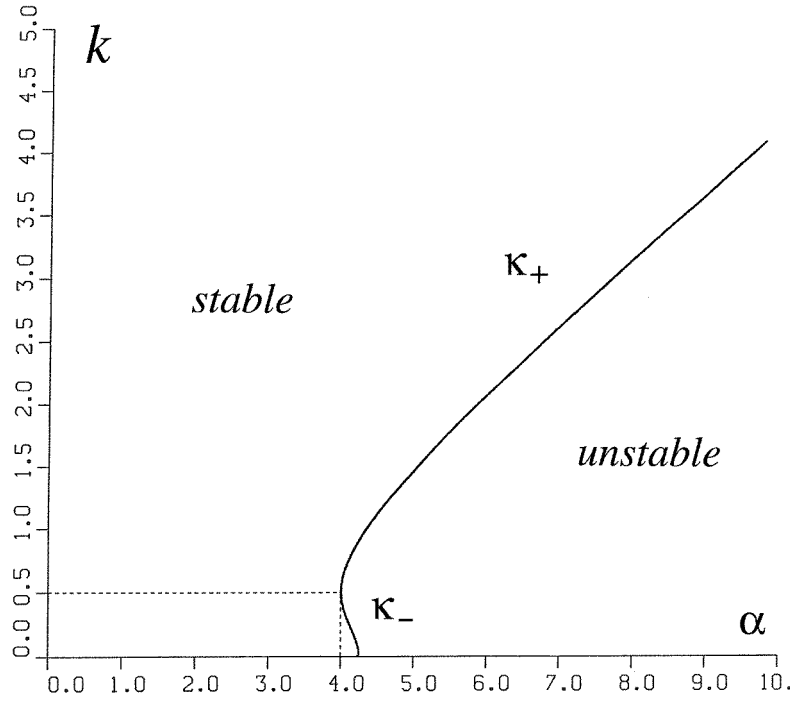


Figure 1. Marginal stability curve $k = \kappa_{\pm}(\alpha)$ for the basic travelling wave solution.

Along the curves $k = \kappa_{\pm}(\alpha)$

$$\omega = \pm \frac{1}{2}i\sqrt{\alpha + 4\alpha\kappa_{\pm}(\alpha)} \neq 0 \quad (3.4)$$

and hence the passage from the stability to instability domain involves a Hopf-type bifurcation, indicating a transition to a time-dependent oscillatory solution.

The basic travelling wave solution becomes unstable as soon as $\alpha \sim N(1 - \sigma)(1 - \gamma^{-1})$ exceeds $\alpha_c = 4$.

It is interesting that for all the distinctions in the underlying physics, the instability criteria for both subsonic and supersonic detonations, adapted for the present SHR approximation [11–15], appear to be quite similar in form. This presumably is due to the fact that the main reason for the instability is a strong disparity between the rates of mass and pressure transfer ($\sqrt{D_{\text{mol}}t} \ll \sqrt{D_b t}, a_0 t$), irrespective of whether the latter is diffusive or acoustic by nature. Here D_{mol} is the molecular diffusivity of the deficient reactant.

4. Free-interface model. Numerical simulations

In this section some results on numerical simulation of the above free-interface model pertinent to the combustion wave progressing through an insulated tube of square cross section

$$0 < \xi < a \quad 0 < \eta < a \quad -\infty < \zeta < \infty \quad (4.1)$$

are presented. In contrast to the original formulation with distributed kinetics (2.1)–(2.4) which requires a high-resolution grid in order to capture the reaction zone, the specifics of the

free-interface model (2.20) and (2.21) make it accessible to effective numerical simulations without turning to supercomputing facilities even in three-dimensional situations.

First we note that equations (2.20) and (2.21) combined with (2.23) lead to the following condition at the interface $\hat{F} = \hat{\xi} - f(\hat{\xi}, \hat{\eta}, \hat{\tau}) = 0$:

$$\Pi^+ = \Pi^- = \Pi \quad \frac{\partial \Pi^+}{\partial \mathbf{n}} - \frac{\partial \Pi^-}{\partial \mathbf{n}} = V \quad Q(\Pi) = V \quad (4.2)$$

where \mathbf{n} is the unit normal to the interface $\hat{F} = 0$, and V is its normal velocity,

$$\mathbf{n} = \frac{(-f_{\hat{\xi}}, -f_{\hat{\eta}}, 1)}{(1 + f_{\hat{\xi}}^2 + f_{\hat{\eta}}^2)^{1/2}} \quad V = \frac{f_{\hat{\tau}}}{(1 + f_{\hat{\xi}}^2 + f_{\hat{\eta}}^2)^{1/2}}. \quad (4.3)$$

The free-interface problem is therefore expressed in terms of the pressure only.

Secondly, due to Darcy's law, the requirement that the tube is insulated results in zero normal components of the pressure gradient at the walls which leads to the following boundary conditions:

$$\Pi_{\xi}(0, \eta, \zeta, \tau) = \Pi_{\xi}(a, \eta, \zeta, \tau) = \Pi_{\eta}(\xi, 0, \zeta, \tau) = \Pi_{\eta}(\xi, a, \zeta, \tau) = 0 \quad (4.4)$$

$$f_{\xi}(0, \eta, \tau) = f_{\xi}(a, \eta, \tau) = f_{\eta}(\xi, 0, \tau) = f_{\eta}(\xi, a, \tau) = 0. \quad (4.5)$$

For the numerical simulation we need to reformulate the problem in terms of the coordinate frame moving with the interface,

$$\tilde{\xi} = \hat{\xi} \quad \tilde{\eta} = \hat{\eta} \quad \tilde{\tau} = \hat{\tau} \quad \tilde{\zeta} = \hat{\zeta} - f(\hat{\xi}, \hat{\tau}) \quad (4.6)$$

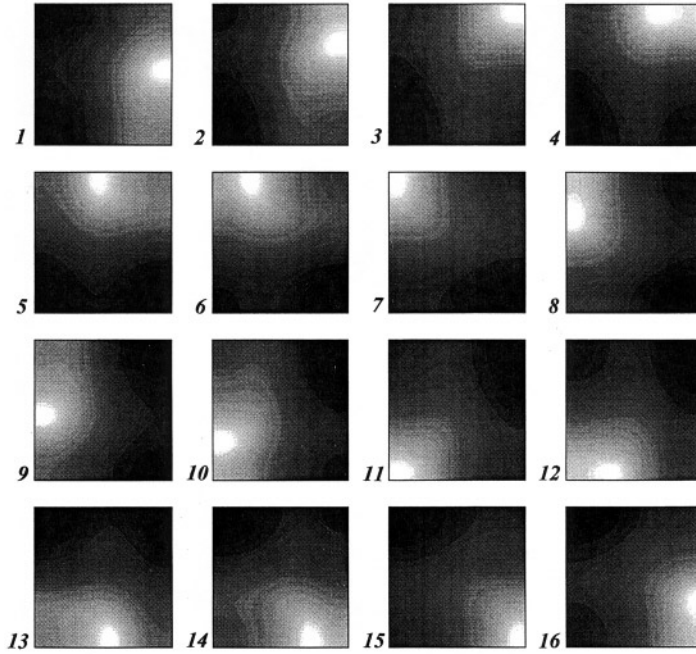


Figure 2. Snapshots of the interface temperature projected onto the (ξ, η) -plane (left to right and downward). Lighter shade corresponds to a higher temperature.

which renders the interface motionless. The free-interface problem in terms of the new coordinates thus becomes

$$\Pi_{\tilde{\tau}} = \Pi_{\tilde{\xi}\tilde{\xi}} + \Pi_{\tilde{\eta}\tilde{\eta}} + (1 + f_{\tilde{\xi}}^2 + f_{\tilde{\eta}}^2)\Pi_{\tilde{\zeta}\tilde{\zeta}} - 2f_{\tilde{\xi}}\Pi_{\tilde{\xi}\tilde{\zeta}} - 2f_{\tilde{\eta}}\Pi_{\tilde{\eta}\tilde{\zeta}} + (f_{\tilde{\tau}} - f_{\tilde{\xi}\tilde{\xi}} - f_{\tilde{\eta}\tilde{\eta}})\Pi_{\tilde{\zeta}} \quad (4.7)$$

$$\Pi^+(\tilde{\xi}, \tilde{\eta}, 0, \tilde{\tau}) = \Pi^-(\tilde{\xi}, \tilde{\eta}, 0, \tilde{\tau}) = \Pi(\tilde{\xi}, \tilde{\eta}, 0, \tilde{\tau})$$

$$\Pi_{\tilde{\eta}}^+(\tilde{\xi}, \tilde{\eta}, 0, \tilde{\tau}) - \Pi_{\tilde{\eta}}^-(\tilde{\xi}, \tilde{\eta}, 0, \tilde{\tau}) = V \quad (4.8)$$

$$Q(\Pi(\tilde{\xi}, \tilde{\eta}, 0, \tilde{\tau})) = -V.$$

The above problem was solved numerically using a simple finite-difference scheme. Our main objective was to establish the existence of spinning detonation and in the current paper we limit our presentation of the three-dimensional numerical results to this regime. Indeed, such a regime can readily be found. Figure 2 represents the evolution of the interface temperature for $a = 4$, $\sigma = 0.2$, $\gamma = 1.4$ which leads to $\Sigma = 0.466$ and $\alpha = 4.2$. The animation should be viewed from left to right and downward with the time interval $\Delta\tau = 0.4$, where each window is a snapshot of the interface temperature projected onto the square cross section with a lighter shade corresponding to the higher temperature. One can easily detect a single hot spot rotating about the perimeter of the square. To make the matter even more transparent we present the view of the four faces of the tube where the edges of the front leave a ‘temperature trace’ as a horizontal axis represents time (figure 3). One can observe a ‘spiral’ formed on the walls of the tube. Note also how the geometry of the domain is manifested in forming a weaker wave in the opposite direction due to a sort of reflection in the corners. The view of the front positions on one of the walls with the time increment $\Delta\tau = 0.4$ (figure 4), completes the picture.

Figure 5 represents a sample of the one-dimensional pulsating front motion (interface velocity versus time) with $\Sigma = 0.466$ and $\alpha = 4.44$. The purpose of this illustration is to compare it with a similar pulsating regime for the original model with distributed reaction (section 5).

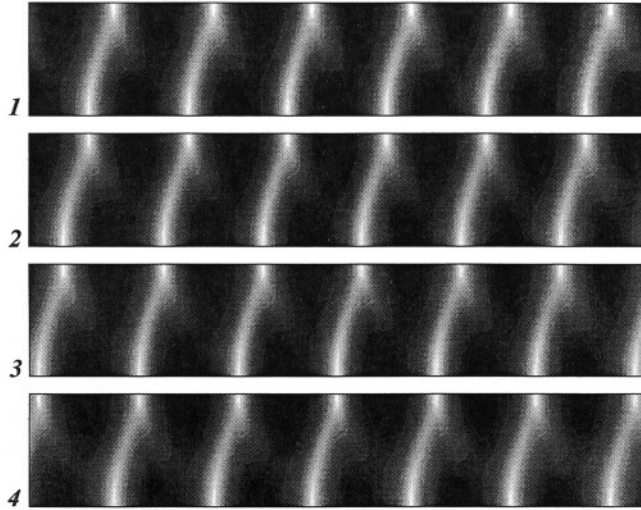


Figure 3. ‘Temperature trace’ of the front on the unfolded external surface of the tube. The horizontal axis represents time. Lighter shade corresponds to a higher temperature.

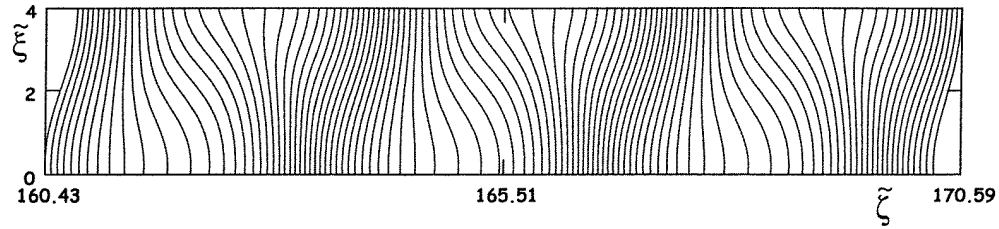


Figure 4. Front positions $\tilde{\zeta} = f(\tilde{\xi}, \tilde{\eta}, \tilde{\tau})$ imprinted on the $(\tilde{\xi}, \tilde{\zeta})$ -wall with time increment $\Delta\tilde{\tau} = 0.4$.

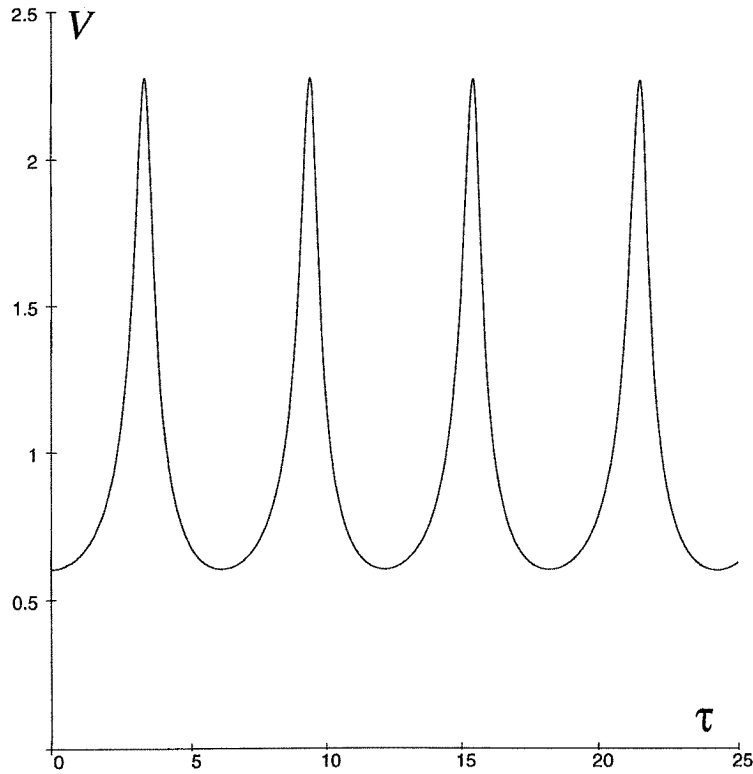


Figure 5. One-dimensional pulsating front motion (interface velocity versus time) with $\Sigma = 0.466$, $\alpha = 4.44$ for the free-interface model.

5. Distributed kinetics

The transition from the distributed kinetics (2.4) to the localized one (2.7) is not an asymptotically rigorous procedure, but rather is an extrapolation allowing one to simplify the original problem and hopefully without any major distortion of its dynamical peculiarities. A comprehensive comparison of the two models is a formidable task far beyond the scope of the present study. To acquire at least some degree of confidence about the adopted approach it is important to ascertain whether the oscillatory propagation is indeed inherent to the original formulation (2.1)–(2.6). To this end a one-dimensional version of the model (2.1)–(2.6) was considered on a semi-infinite interval, $0 < \xi < \infty$, subject to the following initial and boundary

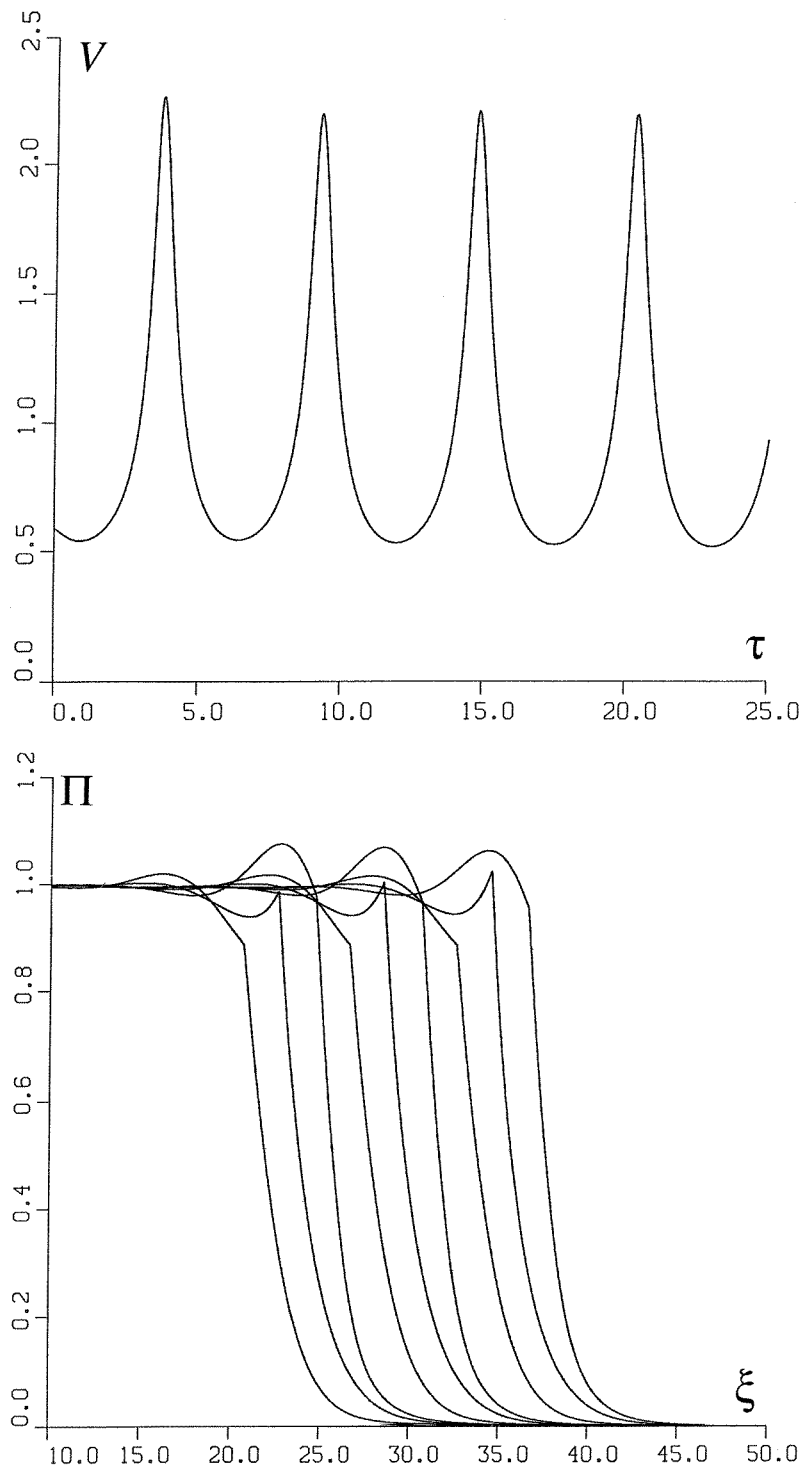


Figure 6. Galloping propagation mode for the model based on the distributed kinetics. Temporal evolution of the reaction wave speed $V(\tau)$ for the well settled solution (a). Profiles of pressure Π (b) and temperature Θ (c) at several consecutive instants of time.

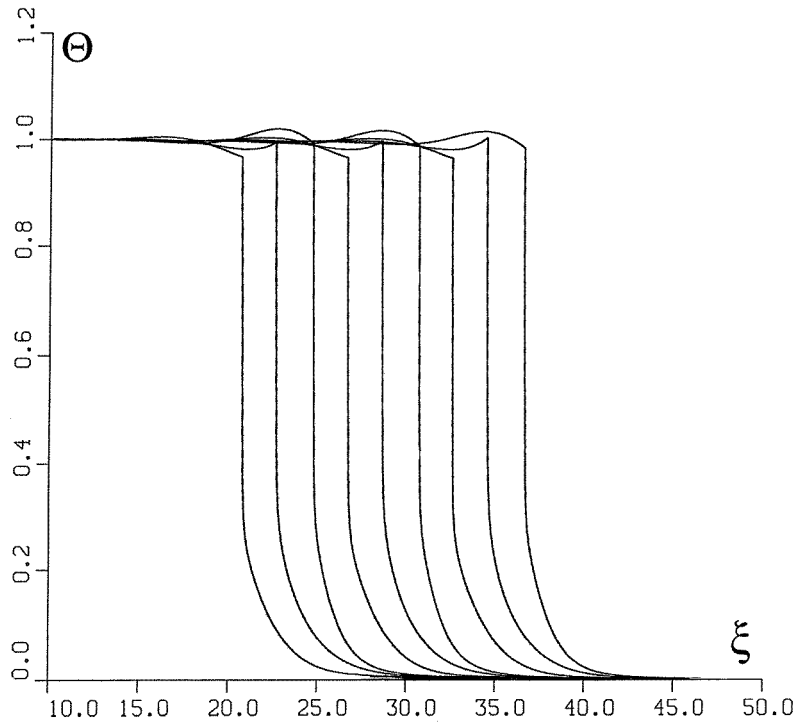


Figure 6. Continued.

conditions,

$$\begin{aligned} \Theta(\xi, 0) &= \exp(-(\xi/\ell)^2) & \Pi(\xi, 0) &= 0 \\ \Phi(\xi, 0) &= 1 \end{aligned} \quad (5.1)$$

$$\begin{aligned} \Theta_\xi(0, \tau) &= \Pi_\xi(0, \tau) = \Phi_\xi(0, \tau) = 0 \\ \Theta(+\infty, \tau) &= 0 & \Pi(+\infty, \tau) &= 0 & \Phi(+\infty, \tau) &= 1. \end{aligned} \quad (5.2)$$

Figure 6 shows results of the corresponding numerical simulation conducted for $N = 6.875$, $\sigma = 0.2$, $\gamma = 1.4$ ($\alpha = 4.27$), $\ell = 1$, i.e. slightly above the stability threshold ($\alpha_0 = 2 + \sqrt{5} \simeq 4.24$) suggested by the analytical estimates (section 3).

After an initial transient period the solution settles into the regime of strictly periodic pulsations, quite similar to those occurring in the free-interface model at α close to α_0 (figure 5).

The problem was solved by a conventional non-adaptive finite-difference method, involving both explicit and implicit codes.

6. Concluding remarks

An important outcome of the presented analysis is the observation that the bifurcations found appear to be totally unrelated to hydrodynamic nonlinearities, absent from the model (e.g. thermal expansion-induced advection). In this connection it would be of great interest to

ascertain whether this is also the case for supersonic detonation. The pertinent reaction–diffusion–acoustics model has already proved itself for a number of problems: the deflagration-to-detonation transition in ducts and the hysteresic transition from supersonic to subsonic detonation [1], the transition to detonation in end-gases and the soft initiation of detonation in non-uniformly preconditioned gases [16]. It would therefore be surprising if the oscillatory propagation were to fall beyond the model’s scope. This intriguing issue will be addressed in forthcoming studies.

Acknowledgments

The work of MF was supported by the NSF grant no DMS-9623006. The work of IB and GS was supported by the DOE grant no DE-FG02-88ER13822, by the US–Israel BSF grant no 9800374, by the Israel Science Foundation under grant no 40-98, by the Israel Ministry of Science under grant no 9685-1-97, by the Belfer Foundation for Energy Research and by the European Community Programmes INTAS-906-1173 and TMR-ERB FMRX CT98 0201 and the Research Foundation of Tel Aviv University (grant no 784). The numerical simulations were performed at the Israel Inter-University Computer Center.

Appendix

This section deals with evaluation of the normalizing factor A (2.4) setting the velocity of the basic solution at unity. The subsequent analysis is a modified and extended version of that given in [8].

The basic solution of the system (2.1)–(2.5) is sought in the form of a travelling wave moving from left to right along the axis ξ , i.e.

$$\Theta = \Theta(s) \quad \Phi = \Phi(s) \quad \Pi = \Pi(s) \quad \text{where } s = \xi - \tau.$$

Thus one ends up with the following problem for ordinary differential equations:

$$-\gamma\Theta_s + (\gamma - 1)\Pi_s = \Omega(\Phi, \Theta) \quad (\text{A.1})$$

$$-\Phi_s = -\Omega(\Phi, \Theta) \quad (\text{A.2})$$

$$-\Pi_s + \Theta_s = \Pi_{ss} \quad (\text{A.3})$$

$$\begin{aligned} \Theta(+\infty) = 0 & \quad \Pi(+\infty) = 0 & \quad \Phi(+\infty) = 1 \\ \Theta_s(-\infty) = 0 & \quad \Pi_s(-\infty) = 0 & \quad \Phi(-\infty) = 0. \end{aligned}$$

It is assumed that the reaction rate at $s = +\infty$ is too small to be reckoned with. Global integration of the equations (A.1)–(A.3) readily implies

$$\Theta(-\infty) = 1 \quad \Pi(-\infty) = 1. \quad (\text{A.4})$$

The system (A.1)–(A.4) is easily reduced to a single equation for the pressure Π ,

$$\gamma\Pi_{ss} + \Pi_s + \Omega(\Phi, \Theta) = 0 \quad (\text{A.5})$$

where

$$\Phi = 1 - \Pi - \gamma\Pi_s \quad \Theta = \Pi + \Pi_s \quad (\text{A.6})$$

$$\Pi(+\infty) = 0 \quad \Pi(-\infty) = 1. \quad (\text{A.7})$$

Considering $R = -\Pi_s$ as a function of Π , the problem (A.5)–(A.7) is reduced to an overdetermined problem for the first-order ordinary differential equation

$$\gamma R R_{\Pi} - R + \Omega(\Phi, \Theta) = 0 \quad (\text{A.8})$$

where

$$\Phi = 1 - \Pi + \gamma R \quad \Theta = \Pi - R \quad (\text{A.9})$$

$$R(0) = 0 \quad R(1) = 0. \quad (\text{A.10})$$

To ensure the existence of a strictly time-independent combustion wave the reaction rate, Ω , should be truncated at low temperatures. One may set, for example,

$$\Omega = 0 \quad \text{at} \quad \Theta < \Theta_* = (\gamma - 1)/4\gamma. \quad (\text{A.11})$$

For high-enough Zeldovich numbers (β) the final result should not depend on the specifics of the truncation.

Below $\Theta = \Pi - R = (\gamma - 1)/4\gamma$, the problem (A.8)–(A.10) yields

$$R = \Pi/\gamma. \quad (\text{A.12})$$

Hence, at the truncation point

$$\Pi = \Pi_* = \frac{1}{4} \quad R = R_* = 1/4\gamma. \quad (\text{A.13})$$

For the subsequent numerical procedure it is useful to represent A as (see (2.6))

$$A = A_0 \exp \left\{ \frac{N}{(\sigma + (1 - \sigma)(1 - \gamma^{-1}))} \right\} \quad (\text{A.14})$$

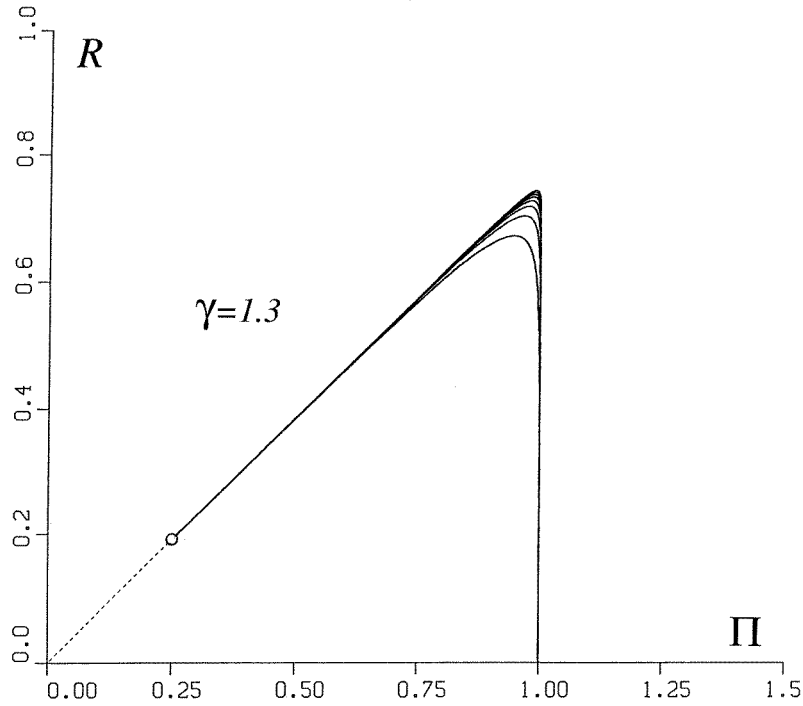


Figure A1. Integral curves $R = R(\Pi)$ for equation (A.8) corresponding to the boundary conditions $R(1) = 0$, $R(\frac{1}{4}) = 1/4\gamma$ and evaluated for several values of the scaled activation energy, β .

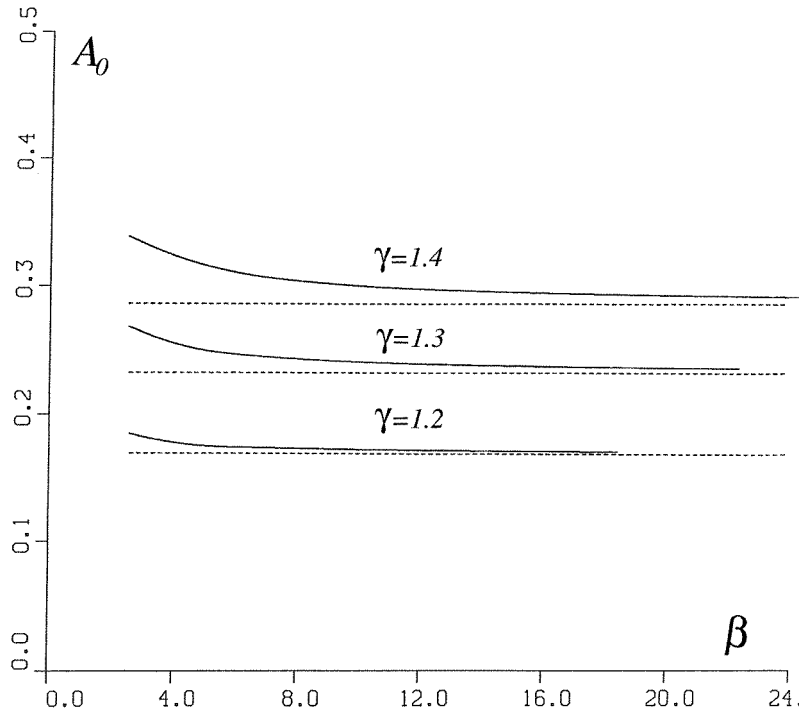


Figure A2. Parameter A_0 versus scaled activation energy β evaluated for $\gamma = 1.4, 1.3, 1.2$ and $\sigma = 0.2$.

thereby recasting Ω into

$$\Omega = A_0 \Phi \exp \left\{ \frac{\beta(\Theta - (1 - \gamma^{-1}))}{(\sigma + (1 - \sigma)(1 - \gamma^{-1}))(\sigma + (1 - \sigma)\Theta)} \right\} \quad (\text{A.15})$$

where $\beta = N(1 - \sigma)$ is the Zeldovich number.

Figure A1 plots the integral curves originating at the point $\Pi = 1, R = 0$ and entering the point $\Pi = \Pi_*, R = R_*$. The calculations were performed for $2 < \beta < 20$ at $\gamma = 1.2, 1.3, 1.4$ and $\sigma = 0.2$. The solution was obtained numerically by a conventional ‘shooting’ method which simultaneously determines A_0 and hence A . The calculated A_0 versus β dependence is shown in figure A2. With increasing β , A_0 gradually approaches $A_0 \simeq 1 - \gamma^{-1}$, quite in line with (A.14).

In principle any specific cut-off pressure Π_* inevitably influences the solution $R(\Pi)$ within the reactive range $\Pi_* < \Pi < 1$. The effect, however, may be regarded as weak if transition from the range $0 < \Pi < \Pi_*$ to $\Pi_* < \Pi < 1$ occurs in a sufficiently smooth manner. This is precisely what one observes for $\Pi_* = \frac{1}{4}$ at $\beta \geq 2.5$. The curves $R(\Pi)$ issuing from the point $\Pi_* = \frac{1}{4}, R_* = \Pi_*/\gamma = 1/4\gamma$ appear as rather smooth continuations of the ray $R = \Pi/\gamma$ coming from the origin (figure A1, broken line).

References

- [1] Brailovsky I and Sivashinsky G I 1997 *Combust. Sci. Technol.* **130** 201–31
- [2] Brailovsky I and Sivashinsky G I 2000 *Combust. Flame* at press

- [3] Lyamin G A and Pinaev A V 1987 *Combust. Expl. Shock Waves* **23** 399–402
- [4] Dimitriou P, Puszanski J and Hlavacek V 1989 *Combust. Sci. Technol.* **68** 101–11
- [5] Bayliss A and Matkowsky B 1990 *SIAM J. Appl. Math.* **50** 437–59
- [6] Margolis S B 1991 *Prog. Energy Combust. Sci.* **17** 135–62
- [7] Frankel M, Roytburd V and Sivashinsky G I 1998 *Combust. Theory Modelling* **2** 479–96
- [8] Brailovsky I, Goldshtein V, Schreiber I and Sivashinsky G I 1997 *Combust. Sci. Technol.* **124** 145–65
- [9] Brailovsky I and Sivashinsky G I 1998 *Combust. Theory Modelling* **2** 429–47
- [10] Goldfarb I, Kuzmenko G and Goldshtein V 1999 *Phys. Lett. A* **251** 394–403
- [11] Sivashinsky G I 1981 *SIAM J. Appl. Math.* **40** 432–8
- [12] Schelkin K I 1966 *Sov. Phys.–Usp.* **8** 780–97
- [13] He L and Clavin P 1995 *C. R. Acad. Sci., Paris II* **320** 635–40
- [14] Clavin P and He L 1996 *J. Fluid Mech.* **306** 353–78
- [15] Clavin P and He L 1996 *Phys. Rev. E* **53** 4778–84
- [16] Brailovsky I and Sivashinsky G I unpublished